Synthesis of PEDOT particles and manufacturing of electrically-conductive PEO / PEDOT thermoplastic composites by twin-screw extrusion

Adèle Karst, Thibault Parpaite, Michel Bouquey, Hervé Pelletier, Jérémie Soulestin, Cédric Samuel

Synthesis of PEDOT particles and manufacturing of electrically-conductive PEO / PEDOT thermoplastic composites by twin-screw extrusion

Adèle Karst [1,2,3], Thibault Parpaite[1,2,*], Michel Bouquey[1], Hervé Pelletier[1,2], Jérémie Soulestin[3], Cédric Samuel[3,*]

[1] Université de Strasbourg, CNRS, Institut Charles Sadron UPR 22, F-67000 Strasbourg, France

[2] INSA Strasbourg

[3] IMT Nord Europe, Institut Mines-Télécom, Univ. Lille, Centre for Materials and Processes, F-59000 Lille, France

*Corresponding author, E-mail: cedric.samuel@imt-nord-europe.fr; thibault.parpaite@ics-cnrs.unistra.fr

Highlights:

- Electrically-conductive PEDOT particles up to 50 $S.cm^{-1}$ were successfully obtained by an oxidative polymerization process
- Polymerization temperature has been identified as the key parameter to obtain highly conductive PEDOT particles and relationships with structural features were explored
- Incorporation of PEDOT particles into a PEO thermoplastic matrix was successfully performed up to 60 wt% by twin screw extrusion
- PEO / PEDOT thermoplastic composites with outstanding electrical conductivities up to 12 $S. cm^{-1}$ were successfully obtained and the electrical percolation is discussed

Abstract: The electrical conductivity of thermoplastic composites made of poly(3,4-ethylenedioxythiophene) (PEDOT) particles and poly(ethylene oxide) (PEO) matrices is here investigated, in particular using a manufacturing process based on twin-screw extrusion. PEDOT particles without PSS were first synthesized by oxidative polymerization in an aqueous medium and characterized using various techniques (conductivity measurements, SEM, TGA, laser granulometry, XRD and XPS). The polymerization temperature of PEDOT particles was found to be a crucial factor. A maximal conductivity of 50 S/cm was obtained when synthesized at ambient temperature. Relationships between the polymerization temperature and the structure of PEDOT particles were revealed and discussed. PEDOT particles were then incorporated up to 60 wt% into PEO matrix by twin-screw extrusion to manufacture electrically-conductive PEO / PEDOT thermoplastic composites. Their electrical conductivity increased with the PEDOT content and outstanding electrical conductivities up to 12 S/cm were reached. The electrical percolation of this system was determined and discussed based on morphological studies by SEM and X-Ray tomography. The effect of PEDOT concentration on thermal properties of PEO matrices was also revealed by DSC. This work provides a novel approach for the manufacture of thermoplastic composites with high electrical conductivities using industrial technologies with multiple applicative perspectives, in particular into polymer-based electronics.

Keywords: Conductive polymers, PEDOT, Polymerization, Composites, Extrusion, Electrical Conductivity

1. INTRODUCTION

The development of electrically-conductive thermoplastic composites represents a longstanding area of research. Indeed these materials are currently implemented in the electronic industry for ESD prevention or EMI shielding of sensitive elements for which electrical conductivities between 10^{-9} to 10^{-3} S/cm are required [1]–[11]. Electrically-conductive thermoplastic composites are envisioned for a broad range of advanced applications such as sensors (strain, pressure, liquid-gas, temperature), wires / interconnects, heaters, antennas, bipolar plates for fuel cells, thermoelectric elements and electrodes / current collectors for batteries and supercapacitors [12]–[23]. The main advantage of electrically-conductive thermoplastic composites lies in their cost-effective and industrially-relevant manufacturing techniques, in particular by solvent-free technologies such as extrusion- and injection-based molding processes. Additive manufacturing technologies also open new design strategies with an optimized 3D integration of the electrical functionality using these thermoplastic composites [24]–[30]. These highly-conductive thermoplastic composites are mandatory for most of advanced applications . However, achieving high electrical conductivity while retaining acceptable mechanical performances and ability of melt-state processing still represents a strategic challenges.

Electrically-conductive thermoplastic composites are usually composed of thermoplastic polymer matrices (mainly polyolefins and engineering polymers) filled with carbon particles (carbon black, graphite, carbon nanotubes, graphene, etc.) and a widely researched topic [1]–[3], [31]–[36]. In order to impart significant electrical conductivity, the amount of carbon fillers needs to be well-above the so-called electrical percolation threshold and twin-screw extrusion techniques are fundamental to produce thermoplastic composites with high amount of conductive fillers. Carbon black or graphite are commonly used at the industrial scale and percolation thresholds close to 5 – 10 wt% in polyolefins matrices are observed with maximal loadings of up to 40 – 50 wt%. Lower percolation thresholds (typically 1 – 2 wt%) and higher electrical conductivities are reached using carbon nanotubes or graphene but their high aspect ratio limits the maximal amount that can be incorporated into thermoplastic polymers due to rheological considerations. As a result, most of electrically-conductive thermoplastic composites produced by twin-screw extrusion exhibit modest electrical conductivities of up to 0.1 – 1 S/cm. It is worth noticing that percolation thresholds and maximal conductivities are affected by multiple parameters such as the initial quality of the carbon filler, its surface chemistry/treatment, the matrix's nature and the extrusion/injection processing conditions. Besides modest electrical performances, several additional aspects regarding these thermoplastic composites are of concerns, in particular (i) their high rigidity and low toughness, (ii) their high prices and (ii) their potential (eco)toxicity (during the manufacturing, use and end-of-life). These aspects clearly restrict their application fields and, therefore, alternative solutions that tackle these challenges are very important and topical.

Intrinsically-conductive polymers clearly represent emerging candidates, in particular poly(3,4-ethylenedioxythiophene) (PEDOT). Outstanding electrical conductivities up 6000 S/cm are reported when PEDOT is combined with poly(styrene sulfonate) (PSS) or other counter-anions [37]–[41]. Additives (NMP, DMSO, etc…) and acidic post-treatments are mandatory to reach such extreme electrical conductivities. PEDOT:PSS aqueous solutions also form highly-transparent and ductile/stretchable films by drop-casting, screen-printing and inkjet-printing. In this respect, PEDOT:PSS is expected to play a key role in future printed electronic systems as light-emitting diodes, field-effect transistors, photovoltaic solar cells, thermoelectric elements, batteries/supercapacitors and (bio)sensors [40]–[50]. However, dried and solid forms of PEDOT:PSS have never been considered as suitable for melt-state extrusion due to infusibility or absence of melting/softening phenomena at relevant temperatures. For this purpose, our research group has recently developed an innovative approach using high-molecular weight poly(ethylene oxide) (PEO) as a melt processing additive for PEDOT:PSS [51]. Their choice of PEO was motivated by its high compatibility with PEDOT:PSS [52], high solubility in aqueous medium and good processability in the melt state. It is also important to consider that PEO can demonstrate a ionic transport and, therefore, can demonstrate some electrical conductivity. For this reason, pure PEO can show an electrical conductivity higher than other polymer matrices. However, this conductivity remains low and the effect of the addition of conductive charges on the electrical conductivity of the composite will be clearly demonstrated in this study. PEO and PEDOT:PSS blends were prepared in aqueous solutions followed by a solvent evaporation step to recover dried films and powders suitable for extrusion and/or thermocompression. Interestingly, dried PEO / PEDOT:PSS films obtained from aqueous solutions displayed high electrical conductivities in the range 100 – 1000 S/cm with a percolation threshold of PEDOT:PSS into PEO close to 8 wt%. Based on morphological and DSC analysis, the good compatibility between these two polymers was confirmed. Extrusion trials were successfully conducted at 100 – 120°C with PEO-based blends containing 10 – 40 wt.% PEDOT:PSS and a maximal electrical conductivity up to 4 S/cm was recorded for extruded films, exceeding by one decade the electrical conductivity of commercial thermoplastic composites based on carbon black or carbon nanotubes. However, two main limitations were noticed. First, aqueous and highly-diluted solutions are difficult to handle with extrusion processes and solvent-free blending protocols are preferable. Then, PEO / PEDOT:PSS blends experience a dramatic drop of their electrical conductivity during the extrusion process and this main issue imposed a post-treatment step of extruded films using sulfuric acid to partially recover their initial electrical conductivity. This phenomenon could be linked to a phase separation phenomenon producing an insulant PSS-rich phase [53]. As a conclusion, the use of high-molecular weight PEO efficiently promote the melt processing of PEDOT:PSS by extrusion and previous issues could be tackled with alternative strategies.

In this context and based on above mentioned works [54], the present study is dedicated to the synthesis of electrically-conductive PEDOT particles (without PSS) and their subsequent dispersion into PEO by twin-screw extrusion to produce highly-conductive thermoplastic composites. In the first part of the paper we have detailed the investigation of the oxidative polymerization of EDOT in water using various oxidants. The impact of the polymerization temperature on the electrical properties of PEDOT particles is evaluated and the relationship with their structural features is examined by various techniques

(SEM, laser granulometry, XRD and XPS mainly). PEDOT particles with electrical conductivity up to 50 S/cm were easily obtained through this process. In a second part of the paper, we discuss about the incorporation of as-produced PEDOT particles into a thermoplastic PEO matrix by twin-screw extrusion. Using this process, thermoplastic composites are easily manufactured up to 60 wt% of PEDOT into PEO. The electrical percolation curve is constructed and the dispersion of PEDOT particles into PEO is subsequently analysed by various techniques (SEM, tomography and DSC). Results indicate that outstanding electrical conductivities up to 12 $S.cm^{-1}$, representing one of the highest electrical conductivities for thermoplastic composites.

2. EXPERIMENTAL SECTION

2.1. Materials

3,4-Ethylenedioxythiophene (EDOT, 99%, Acros Organics), iron(III) sulfate hydrate ($Fe_2(SO_4)_3$, 97%, Sigma-Aldrich), iron(III) chloride ($FeCl_3$, 97%, Sigma-Aldrich), sodium dodecyl sulfate (SDS, 98.5%, Sigma-Aldrich) were used as received for the synthesis of PEDOT particles by oxidative polymerization. Poly(ethylene oxide) (PEO, 100,000 g/mol, Sigma-Aldrich) was used as received for the production of PEO / PEDOT composites by twin-screw extrusion.

2.2. Synthesis of PEDOT particles in water by oxidative polymerization of EDOT

The synthesis of PEDOT was performed by oxidative polymerization of EDOT and was inspired by the work of Jiand *and al.* [55]. SDS (0.00056 mol) was dissolved into 100 mL of demineralized water. EDOT (0.007 mol) was added dropwise into the previous aqueous solution and the solution was stirred for 2 hours. Oxidant ($Fe_2(SO_4)_3$ or $FeCl_3$, 0.023 mol) was added into the solution. The solution was then placed under magnetic stirring at the desired polymerization temperature (20, 50°C or 80°C) during 48h. The polymerized solution was then centrifuged (9000 rpm, 23 min) to recover a dark blue powder (**Figure 1**), a characteristic color of PEDOT. The powder was then washed and centrifuged two times with acetone:methanol (3:10) and then with ethanol:water (1:1). The powder was finally dried at 60°C for 48 hours. The gravimetric yield of the PEDOT synthesis was determined by **Equation 1**.

$$\text{Gravimetric Yield (\%)} = \frac{m_{PEDOT}}{m_{EDOT} + m_{oxidant} + m_{surfactant}} \quad (1)$$

With m_{PEDOT} the final weight of PEDOT particles recovered after the polymerization – purification procedure, m_{EDOT} , $m_{oxidant}$ and $m_{surfactant}$ the initial weight of EDOT, oxidant and SDS used for the synthesis.

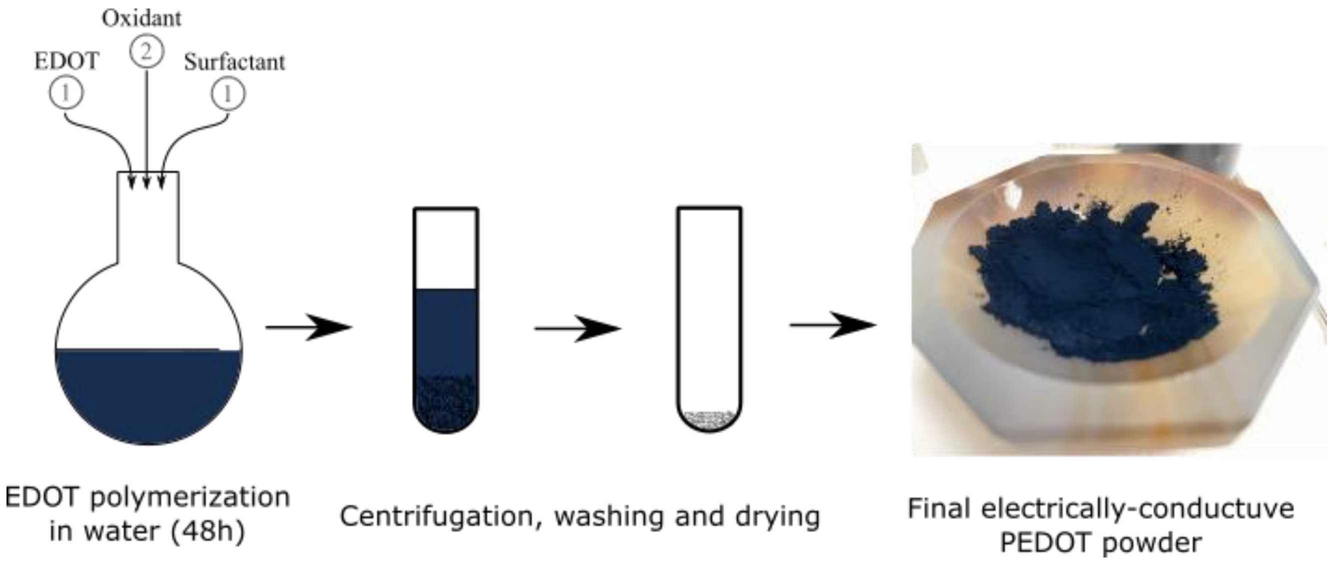

Figure 1: Schematic representation of the EDOT polymerization process for the production of electrically-conductive PEDOT particles.

2.3. Manufacturing of PEO / PEDOT composites by twin screw extrusion

PEDOT particles and the PEO powder were thoroughly mixed using a mortar with a weight ratio of PEDOT ranging from 10 to 60 wt %. Dry-blended powders were then introduced into a twin-screw extruder (Haake Minilab 2, Thermofisher Scientific) operating at a temperature of 80°C and a screw speed of 30 rpm. The extruder was used in direct extrusion mode (residence time close to 1 min) with a rectangular die to produce rectangular ribbons (approx. 3.5 – 4 mm in width and 500 – 900 in thickness µm).

2.4. Characterizations

2.4.1. Measurement of the electrical conductivity

PEDOT powders were first converted into dense pellets using a hydraulic press (45 bars for 30 seconds). Pellets with diameters close to 13 mm were obtained and their thicknesses measured with a precision calliper. Extruded PEO / PEDOT ribbons were cut to a length close to 13 mm and their widths / thicknesses were also measured with a precision calliper. PEDOT pellets and extruded PEO / PEDOT composites were then placed into a homemade four-probes resistance measurement device (**Figure 2**). The device consisted in four aligned probes placed at a distance of 1.8 mm from each other. Probes were mounted on springs to insure a constant pressure during electrical measurements. The current was injected between the two outer probes and the voltage / resistance measured between the two inner probes using an Agilent 34461A multimeter. Resistance was converted into electrical resistivity (ρ) (or conductivity, σ) using **Equation 2**. The determination of the shape factor G is fundamental and values could be found in the work of Topsoe H. [56].

$$\rho = \frac{1}{\sigma} = \mathrm{G}\ \frac{\mathrm{V}}{\mathrm{I}} \qquad (2)$$

with *I* the current injected between the two outer probes, *V* the voltage measured between the two inner probes and *G* being a correction factor depending on sample shape, sample dimensions and arrangement of the electrical contacts.

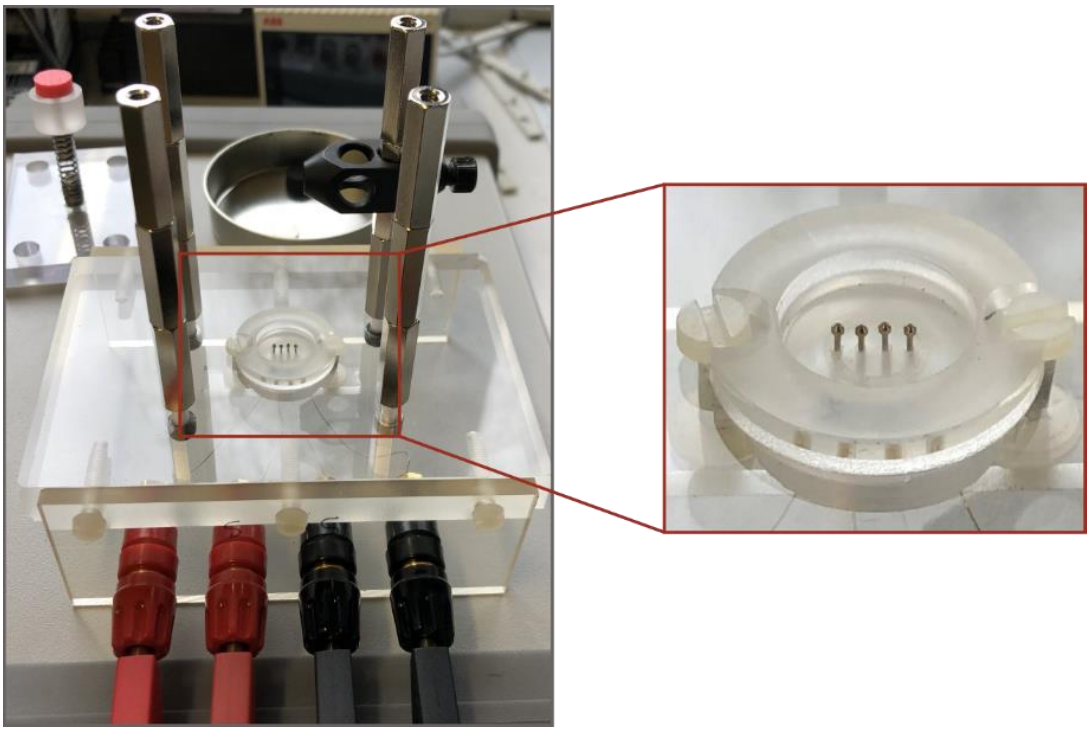

Figure 2: Illustration of the homemade four-probes resistance measurement device.

For cylindrical samples such as PEDOT pellets, the shape factor G depends on sample thickness (t), sample diameter (d, 13 mm in our case) and distance between probes (s, 1.8 mm in our case). If $\mathrm{t} < s/2$, the shape factor G is given by **Equation 3** with C_0 being a constant parameter equals to 0.8665. If $\mathrm{t} > s/2$, the shape factor G is given by **Equation 4** with T_2 being a parameter found in [56] as a function of the ratio t/s.

$$\mathrm{G} = \frac{\pi}{\ln 2}\,\mathrm{t}\,\mathrm{C}_0 \qquad (3)$$

$$\mathrm{G} = \frac{\pi}{\ln 2}\,\mathrm{t}\,\mathrm{T}_2 \qquad (4)$$

For parallelepipedal samples such as extruded PEO / PEDOT ribbons, the shape factor G depends on the sample's length (a, 13 mm in our case), sample's with (b), sample's thickness (t) and distance between probes (s, 1.8 mm in our case). The shape factor G is given by **Equation 5** with R_1 being a parameter found in [56] as a function of the ratios b/s and a/b.

$$G = \frac{\pi}{\ln 2}\, t\, R_1 \qquad (5)$$

2.4.2. Thermal analysis

PEDOT particles were analysed by thermogravimetric analysis (TGA) to evaluate their thermal stability. TGA was carried out on a TGA2 apparatus (Mettler Toledo) under air gas flow at a heating rate of 10°C/min from room temperature to 800°C with an isothermal step at 100°C during 60 min. Extruded PEO / PEDOT composites were analyzed by differential scanning calorimetry (DSC) to evaluate thermal transitions (crystallisation and melting of PEO mainly). DSC was carried out on a DSC25 apparatus (TA Instrument) under air gas flow at a heating rate of 10°C/min from 30°C to 200°C.

2.4.3. Morphological analyses by SEM, laser granulometry and X-Ray tomography

The morphology of PEDOT powders and extruded PEO / PEDOT ribbons were primarily analysed by scanning electron microscopy (SEM, Hitachi SU 8010). Extruded ribbons were fractured in liquid nitrogen for a better observation of their inner structure. Complementary morphological analyses were conducted. PEDOT powders were analysed by laser granulometry using a LS 13230 analyser (Coulter Beckmann Co.) to evaluate their particle size distribution. Extruded ribbons were submitted to X-ray tomography on a EasyTom 150/160 apparatus (RX Solution, tension 100 kV, space resolution 5 µm) for a better visualisation of the aggregation state of PEDOT particles into PEO.

2.4.4. Structural analyses by XRD and XPS

The structure of PEDOT particles was also analysed by X-Ray diffraction (XRD) on the SWING beamline of the SOLEIL synchrotron (Saint-Aubin, France) at a beam energy of 16 keV. The sample-to-detector distance was 6.217 and 0.517 m, respectively, covering a total scattering vector range of $0.00016 < q < 0.25\ nm^{-1}$. The beam size was approximately $500 \times 200\ \mu m^2$. All measurements were performed at room temperature (22°C). The scattered signal was recorded by an Eiger 4 M detector (Dectris Ltd., Switzerland) with a pixel size of 75 µm, in 2 x 2 binning configuration.

The structure of PEDOT particle was also analysed by X-Ray photoelectron spectroscopy (XPS) carried out in an ultrahigh vacuum (base pressure 5.10^{-9} mbar) composed of several interconnected chambers. The analysis chamber was equipped with a RESOLVE 120 MCD5 hemispherical electron analyzer and a dual-anode source (Mg/Al). The sample were mounted on the sample holders using conductive double-sided carbon adhesive tapes. No treatment was applied on the samples before or during measurements. For the XPS measurements, the non-monochromatic MgKα line at 1253.6 eV was used. A survey scan was initially acquired to determine the elements present on each sample. This was followed by high resolution scans of the major element lines. The constant pass energy mode with pass energies of 100 and 20 eV was used to record survey and high-resolution spectra respectively. The Casa XPS 2.3.23 software was used for the analysis of the data in all cases. The error in the measured / calculated binding energy values was estimated around ±0.05 eV.

3. RESULTS & DISCUSSION

3.1. Gravimetric yield and electrical conductivity of PEDOT particles

The production of electrically-conductive PEDOT particles suitable for the manufacturing of thermoplastic composites by extrusion was attempted by oxidative polymerization of EDOT in water without PSS. EDOT is a translucid liquid with a poor solubility in water and aqueous emulsions of EDOT stabilized by SDS were first produced. Then, the introduction of oxidants ($Fe_2(SO_4)_3$ or $FeCl_3$) into the emulsions was followed by a quick change of colour to dark blue, a phenomenon consistent with the polymerization of EDOT into PEDOT turning the initial emulsion into a suspension of PEDOT particles. Dried PEDOT powders were recovered by centrifugation – washing steps and submitted to various analyses, in particular electrical characterizations. **Figure 3** displays the electrical conductivity of the PEDOT powders as a function of the polymerization temperature for the two oxidants. Corresponding gravimetric yields are also given in **Figure 3**. The gravimetric yield was observed to be significantly influenced by the polymerization temperature. High polymerization temperatures improved the gravimetric yield. The same trend was observed with the two oxidants and these results are consistent with those obtained by Jiang *and al.* [57]. However, the electrical conductivity of PEDOT particles drastically decreased with the polymerization temperature and low temperatures favoured the production of highly-conductive PEDOT particles with an interesting electrical conductivity of 47 S/cm obtained for PEDOT particles synthesized at 20°C with $Fe_2(SO_4)_3$. A lower electrical conductivity was observed using $FeCl_3$ at a low polymerization temperature but the negative impact of the polymerization temperature was seen to be less marked with this oxidant. These results are consistent with the work of *Cao et al.* [58] which showed a similar impact of polymerisation temperature on the electrical conductivity of PEDOT. As a conclusion, PEDOT particles with high electrical conductivities could be easily produced at low polymerization temperatures (20°C) and further investigations were conducted to determine the structure of the PEDOT particles and understand the link with polymerization conditions (temperature, oxidant type) and final electrical performances.

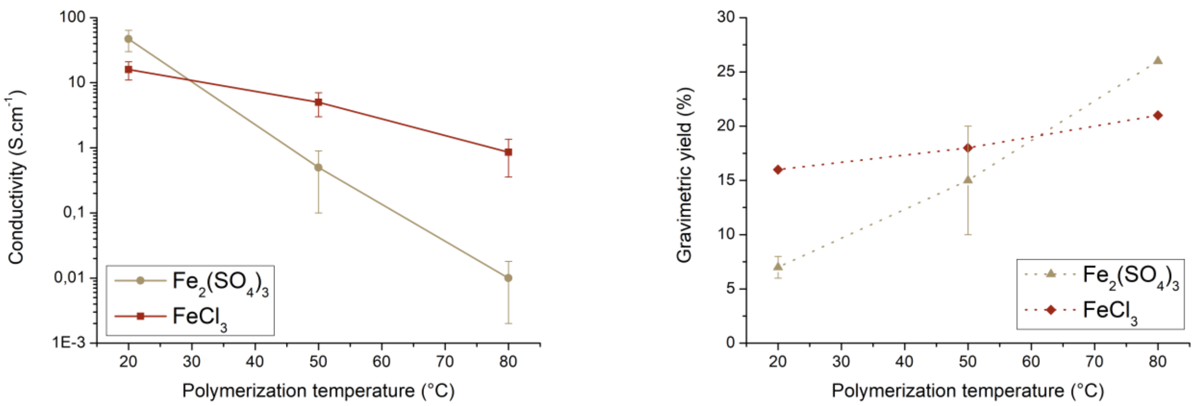

Figure 3: Electrical conductivity of PEDOT particles as a function of the polymerization temperature for the two oxidants, *i.e.* $Fe_2(SO_4)_3$ and $FeCl_3$ (left). Corresponding gravimetric yields (right).

3.2. Morphological analysis of PEDOT particles

The morphology of PEDOT particles synthesized at various polymerization temperatures was first analysed by SEM and **Figure 4** displays the morphology of PEDOT particles synthesized at 20°C, 50°C and 80°C with $Fe_2(SO_4)_3$. All PEDOT particles show similar irregular "cauliflower" morphologies with a high aggregation / agglomeration state, in agreement with previous studies [59], [60]. The sizes of PEDOT particles are difficult to evaluate by SEM and a poor impact of the polymerization temperature is noticed. To get a relevant size analysis, PEDOT powders were redispersed into water and submitted to laser granulometry. **Figure 4** also displays the size distribution of PEDOT particles synthesized with $Fe_2(SO_4)_3$ at various temperatures. The characteristic diameters (d_{10}, d_{50} and d_{90}) are tabulated in **Table 1**. The diameter of PEDOT particles obtained at 20°C and 50°C is comprised between 5 – 50 µm with average value close to 21 – 23 µm. A monomodal distribution is observed and, by comparison with SEM analysis, current PEDOT particles could correspond to aggregates of primary highly-bonded PEDOT particles. For higher polymerization temperatures (80°C), similar diameters are measured but two populations of PEDOT particles are attested. As a conclusion, PEDOT powders consist of micro-scale PEDOT particles with an irregular shape but their sizes are clearly suitable for the processing of thermoplastic composites by extrusion. The polymerization temperature showed no clear impact on the morphology of PEDOT particles and thus structural characterizations were conducted.

Table 1: Characteristic diameters (d_{10}, d_{50} and d_{90}) of PEDOT particles synthesized with $Fe_2(SO_4)_3$ at various polymerization temperatures (analysed by laser granulometry).

	Polymerization temperature		
	20°C	**50°C**	**80°C**
d_{10} (µm)	7.8 ± 0.1	10.5 ± 0.1	4.6 ± 0.4
d_{50} (µm)	21.4 ± 0.2	23.0 ± 0.0	14.0 ± 0.1
d_{80} (µm)	47.5 ± 0.3	41.3 ± 0.6	42.7 ± 0.3

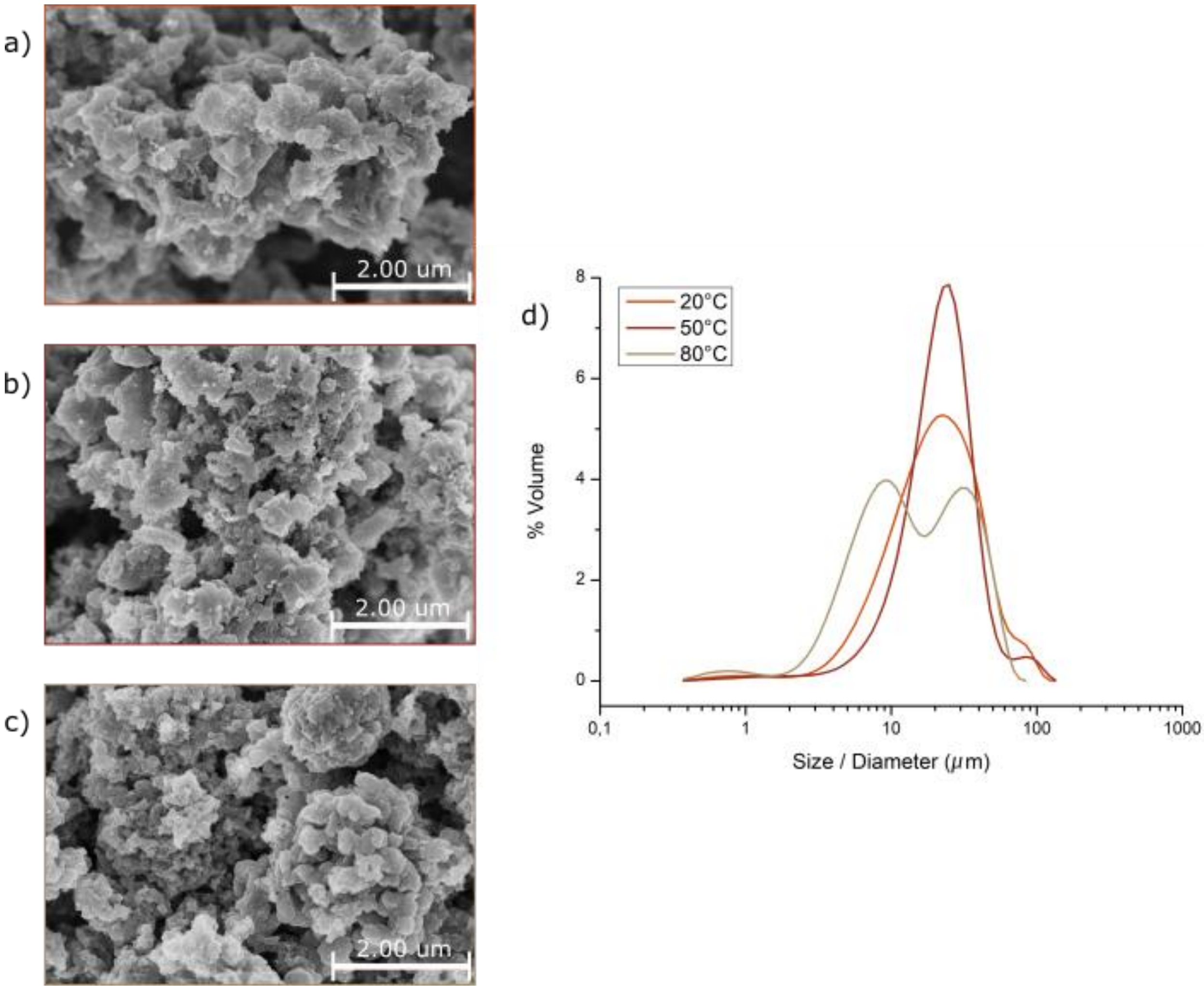

Figure 4: SEM analysis of PEDOT particles synthesized with $Fe_2(SO_4)_3$ at various polymerization temperatures, *i.e.* 20°C (a), 50°C (b) and 80°C (c). Size distribution of PEDOT particles synthesized with $Fe_2(SO_4)_3$ at various polymerization temperatures (analysed by laser granulometry).

3.3. Structural analysis of PEDOT particles

PEDOT micron-scale particles with an irregular shape could be produced irrespective of in any polymerization conditions, however, the impact on electrical conductivity was seen. In this respect, structural analyses were performed to explain the observed trends in terms of electric conductivity. **Figure 5** displays X-Ray diffraction patterns for PEDOT particles synthesized at various polymerization temperatures with $Fe_2(SO_4)_3$. For PEDOT particles synthesized at 20°C, the three main diffraction peaks of PEDOT at 0.045 nm^{-1}, 0.089 nm^{-1} and 0.182 nm^{-1} are clearly detected [37], [61]–[63]. Few impurities seems to be present in this sample but overall PEDOT particles with a good purity could be obtained.

The diffraction patterns of PEDOT particles synthesized at 50°C and 80°C also present the characteristics peaks of PEDOT but numerous side peaks were also found. The latter could be linked to the presence of iron sulfate residues trapped in PEDOT particles and an identification is possible [64] [65], [66]. For PEDOT particles synthesized at 50°C, the impurity seems to be a crystalline form of Fe(II) sulfate, in particular the szomolnokite phase $Fe(SO_4).H_2O$. For PEDOT particles synthesized at 80°C, this crystalline form of Fe(II) sulfate is also found in association with the rozenite phase $Fe(SO)_4.4H_2O$. The presence of iron(II) sulfates in PEDOT particles is in agreement with polymerization mechanisms of EDOT [37] but the amount of iron(II) impurities trapped in PEDOT particles clearly increases with the polymerization temperature. Such phenomenon could create insulant phases into the conductive PEDOT particles and could be responsible for the dramatic drop of the electric conductivity of PEDOT particles produced at elevated temperatures.

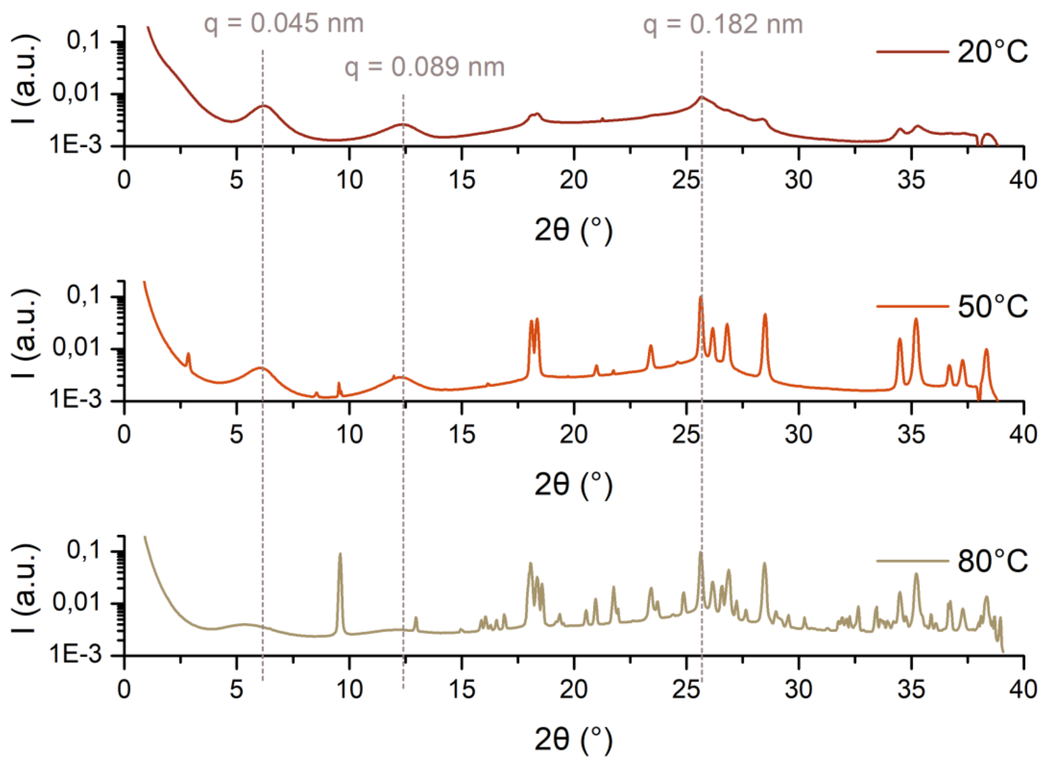

Figure 5: X-Ray analysis of PEDOT particles polymerized at various temperatures with $Fe_2(SO_4)_3$.

The three main diffraction peaks of PEDOT were specifically analysed, in particular their positions and widths. These broad diffraction peaks arise from the presence of low-order crystalline domains of PEDOT and are linked to periodic structures in crystalline regions [37], [61]–[63]. A schematic illustration is proposed in **Figure 6** to highlight the packing of PEDOT chains in crystalline regions with three axis assigned to periodic lamellar stacking (a-axis), periodic π-π stacking (b-axis) and periodic thiophene monomer repetition (c-axis) [37], [61]–[63]. Characteristic distances d_{xyz} could be deduced from the peak position using the Bragg law and crystal dimensions (in the a, b and c-directions) could be calculated from the peak half-width by the Scherrer's equation. The peak located at 0.182 nm^{-1} corresponds to (020) reflections linked to periodic π-π stackings along the b-axis with a characteristic distance d_{020} close to 0.32 nm^{-1}, in agreement with recent reports [62], [63]. This peak could not be analysed for PEDOT particles synthesized at 50°C and 80°C due to a strong overlapping with iron(II) impurities but other peaks located close to 0.045 nm^{-1} and 0.089 nm^{-1} are of good interest. Actually, these two peaks correspond to (200) and (100) reflections linked to the periodic lamellar stackings along the a-axis with characteristic distances d_{200} and d_{100} respectively. The precise position of these peaks and their widths is clearly modified with the polymerization temperature of PEDOT particles. The lamella stacking distances d_{100} and the crystal widths τ_a are tabulated in **Table 2** as a function of the polymerization temperature for PEDOT particles synthesized with $Fe_2(SO_4)_3$. The lamellar stacking distances d_{100} slightly decreases at low polymerization temperature from 1.51 nm at 80°C to 1.44 nm at 20°C. These values are consistent with various values found in literature for highly-conductive PEDOT films produced without PSS and doped with hydrogenosulfonate HSO_4^- counter-anions (d_{100} close to 1.4 nm) [62], [63]. Our results are consequently in agreement with the presence of HSO_4^- counter-anions, as expected by the current polymerization mechanisms of EDOT [37]. The results also suggest that crystalline regions in PEDOT particles are denser for low polymerization temperature and / or contain less defects. Concerning the crystallite size, a clear increase is attested at low polymerization temperature from 1.3 nm at 80°C to 2.3 nm at 20°C. In this respect, a correlation between the electrical conductivity of PEDOT particles and the crystal quality could be concluded, in particular with the crystallite size. The increase of the latter can partially explain the high electrical conductivity obtained for PEDOT particles synthesized at low polymerization temperature, along with a reduced amount of iron(II) crystalline impurities. Here, it can be finally mentioned that the crystallite size of PEDOT particles synthesized at low polymerization temperature seems to be much lower that regular values reported for highly-conductive PEDOT films doped with hydrogenosulfonate HSO_4^- counter-anions [62], [63]. This parameter seems to be of high importance to reach extreme electrical conductivity but the doping rate of PEDOT particles also needs to be considered.

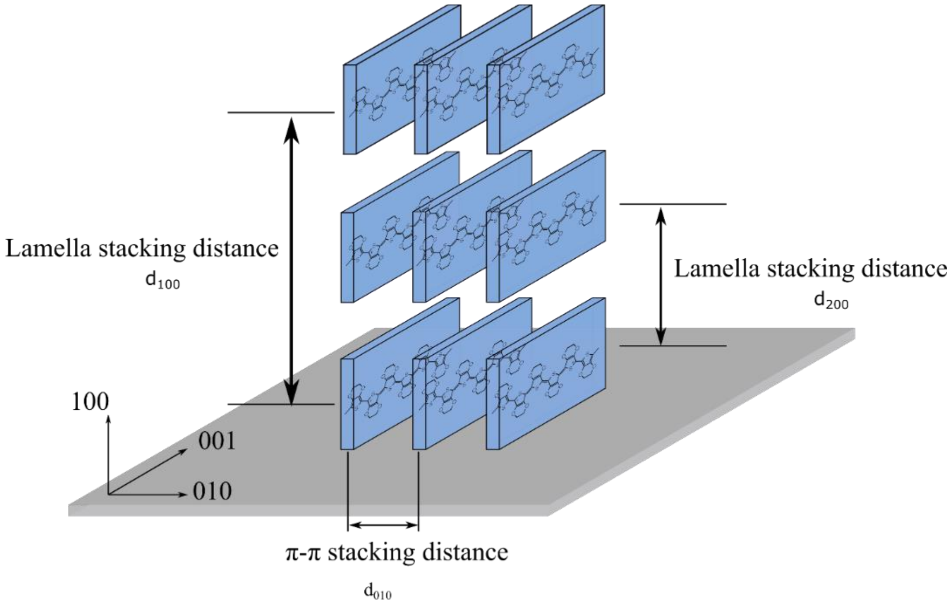

Figure 6: Schematic illustration of the periodic stacking of PEDOT chains within the crystalline phase and relations with characteristic distances obtained from XRD profiles.

Table 2: Crystalline parameters as a function of the polymerization temperature for PEDOT particles synthesized with $Fe_2(SO_4)_3$.

Polymerization temperature	**Conductivity ($S.cm^{-1}$)**	**Peak localization (100) (nm^{-1})**	**Lamellar stacking distance d_{100} (nm)**	**Crystallite size in the a-direction τ_a (nm)**
20°C	47	0.044	1.44	2.3
50°C	0.5	0.043	1.46	1.9

80°C	0.04	0.042	1.51	1.3

The doping rate of PEDOT particles by hydrogenosulfate HSO_4^- or chlorine Cl^- counter-anions could be quantified by XPS [37], [61]–[63], [67]–[72]. The atomic composition of PEDOT particles synthesized at 50°C with $Fe_2(SO_4)_3$ and $FeCl_3$ was first evaluated (**Table 3**). The presence of carbon, oxygen, sulfur, chlorine and iron atoms is highlighted. For PEDOT particles synthesized with $FeCl_3$, carbon-to-oxygen and carbon-to-sulfur ratios are in good agreement with expected ratios for PEDOT. Iron / chlorine atoms are linked to $FeCl_2$ impurities and the excess of chlorine could attest for Cl^- counter-anions with a potential doping rate close to 25% (*i.e.* ratio between PEDOT sulfur atoms and excess chlorine). An amount of $FeCl_2$ impurities close to 16 wt% is also calculated. For PEDOT particles synthesized with $Fe_2(SO_4)_3$, carbon-to-oxygen and carbon-to-sulfur ratio are clearly modified with excess oxygen and sulfur. Excess oxygen and sulfur along with the presence of iron here are linked to $Fe(SO_4)$ impurities and hydrogenosulfate HSO_4^- counter-anions. The doping rate of PEDOT by hydrogenosulfate HSO_4^- counter-anions is estimated to be close to 20% with an amount of $Fe(SO_4)$ impurities close to 26 wt%. It can be mentioned that these figures have a poor precision because calculations are based on the amount of iron, chlorine and sulfur atoms with low XPS responses. An alternative approach is based on high-resolution XPS analysis of the S2p spectra with a specific focus on the S2p peaks of thiophenes (**Figure 7**) [69]–[72]. Actually, the broad peak located between 162 and 168 eV is related to neutral thiophene sulfurs $S^n_{thiophene}$ ($2p_{1/2}$ and $2p_{3/2}$ peaks at 163.6 eV and 164.8 eV) and cationic thiophene sulfurs $S^+_{thiophene}$ ($2p_{1/2}$ and $2p_{3/2}$ peaks at 165.6 eV and 166.8 eV). A convolution of four peaks is consequently expected with a potential determination of the amount of cationic thiophene sulfurs $S^+_{thiophene}$ involved in electrostatic interactions with counter-anions. Deconvolutions indicate that the ratio of cationic thiophene sulfurs $S^+_{thiophene}$ could be in the range 18 – 19% for PEDOT particles synthesized at 50°C either with $Fe_2(SO_4)_3$ and $FeCl_3$ (**Table 3**). A low precision is also expected for this method due to a complex deconvolution procedure but these figures are in agreement with doping rates obtained from XPS atomic compositions. Doping rates between 15 – 25% with electrical conductivities in the range 1 – 10 S/cm are also in agreement with some reports on PEDOT polymerization without PSS using ammonium persulfate initiators [69]. However, many discrepancies are observed within the specialized literature concerning the relationship between doping rate and electrical conductivities because extreme electrical conductivities (in the range 100 – 10000 S/cm) are also observed with 25 – 40% of hydrogenosulfate counter-anions [37], [61]–[63], [67], [68]. In this respect and according to our XRD / XPS analysis, the doping rate does not fully control the final electrical conductivities of PEDOT-based materials and the crystalline structuration of PEDOT seems to be of prime importance to reach extreme conductivities. As a conclusion, PEDOT particles with high electrical conductivities up to 47 S/cm are easily synthesized in water and micron-sized powders suitable for the manufacturing of electrically-conductivity thermoplastic composites are obtained by extrusion. Low polymerization temperatures have a strong positive impact on electrical properties and this effect is probably linked to the size / amount of the PEDOT crystals and amount of impurities.

Table 3: Atomic composition evaluated by XPS, potential doping rate and amount of impurities for PEDOT particles synthesized at 50°C with $Fe_2(SO_4)_3$ and $FeCl_3$.

Oxidant	**C (%)**	**O (%)**	**S (%)**	**Cl (%)**	**Fe (%)**	**Doping rate (%)**	**Impurities** (wt%)
$FeCl_3$	61	23	8	6	2	$18^a – 25^b$	16
$Fe_2(SO_4)_3$	47	40	10	0	3	$19^a – 20^b$	26

[a] Estimated by XPS using the area of cationic $S^+_{thiophene}$ peaks ($2p_{1/2}$ and $2p_{3/2}$ electrons at 165.6 eV and 166.8 eV) and neutral $S_{thiophene}$ peaks ($2p_{1/2}$ and $2p_{3/2}$ electrons at 163.6 eV and 164.8 eV) of the PEDOT backbone.
[b] Estimated by XPS using atomic composition, $FeCl_2$ or $FeSO_4$ impurities are assumed.

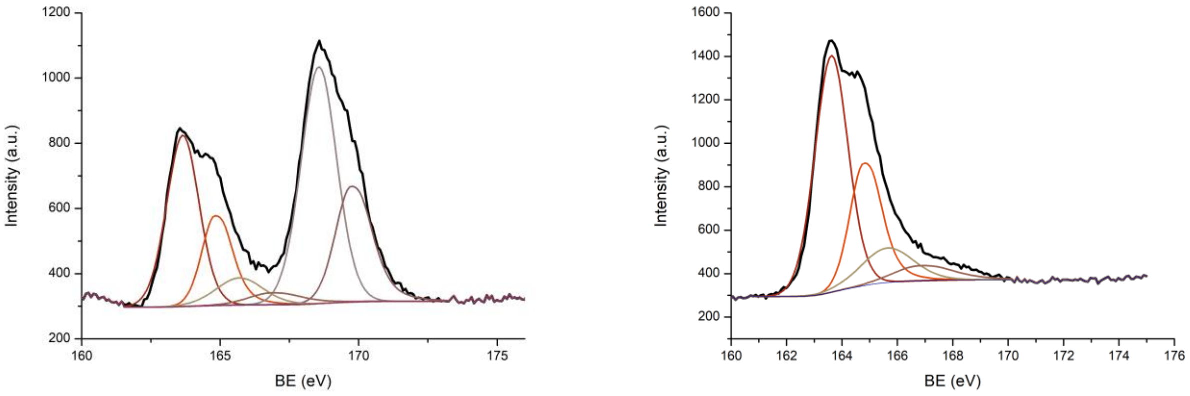

Figure 7: High-resolution S2p spectrum of PEDOT particles synthesized at 50°C with $Fe_2(SO_4)_3$ (left) and $FeCl_3$ (right).

3.4. Electrical percolation in PEO / PEDOT composites manufactured by extrusion

Electrically-conductive thermoplastic composites were manufactured by twin-screw extrusion and PEDOT particles with the highest electrical conductivities (47 S/cm) were selected, *i.e*. PEDOT particles synthesized at 20°C with $Fe_2(SO_4)_3$. Based on previous works by our group, PEO with a molecular weight of 100,000 g/mol was selected as the thermoplastic matrix [51]. We specifically considered the processing window of the thermoplastic composites. Theoretically, the minimal temperature for extrusion processing of such thermoplastic composites should correspond to the melting temperature of the PEO matrix generally observed in the range 55 – 65°C. For rheological reasons, the extrusion processing of high molecular weight PEO is regularly performed at 80 – 120°C. Concerning the maximal processing temperature, the thermal stability of PEDOT is the main aspect to consider. In this respect, a thermogravimetric analysis was performed on the PEDOT particles in order to determine their degradation temperature (**Figure 8**). Residual water is first eliminated with an isothermal step at 100°C and particles are heated to 800°C at 10°C/min. An intense thermal degradation appears at 250°C. The particle seems to be thermically-stable at classical processing temperatures of PEO and the maximal processing temperature of PEDOT particles is estimated close to 170 – 180°C, corresponding to the temperature at 1% mass loss.

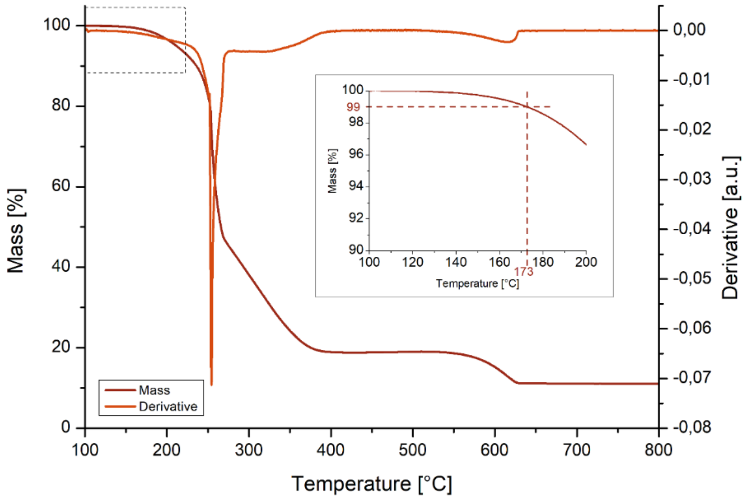

Figure 8: Thermogravimetric analysis (TGA) of PEDOT particles synthesized at 20°C with $Fe_2(SO_4)_3$.

Twin-screw extrusion processing of PEO / PEDOT composites was consequently performed at 80°C without any risk of material degradation. In order to determine the electrical percolation threshold and the maximal conductivity, extrusion experiments were designed with various amount of PEDOT particles from 10 wt% to 60 wt%. It can be noticed that all these thermoplastic composites are easy to transform into extruded ribbon by twin-screw extrusion but higher PEDOT loadings led to a dramatic increase of the viscosity with strong processing difficulties. The electrical conductivity of PEO / PEDOT thermoplastic composites was then evaluated and the impact of the PEDOT content has been displayed in **Figure 9**. Up to 20 wt% of PEDOT, the electrical conductivity of PEO / PEDOT composites roughly remains constant in the range 10^{-4} $S.cm^{-1}$. The electrical conductivity significantly starts to increase for 30 wt% of PEDOT and a maximal electrical conductivity close to 12 $S.cm^{-1}$ is obtained for PEO / PEDOT thermoplastic composites with 60 wt% of PEDOT particles, in agreement with the electrical conductivity of PEDOT particles. To the best of our knowledge, this highly-filled thermoplastic composite developed by twin-screw extrusion display one of the highest electrical conductivities reported in the literature to date.

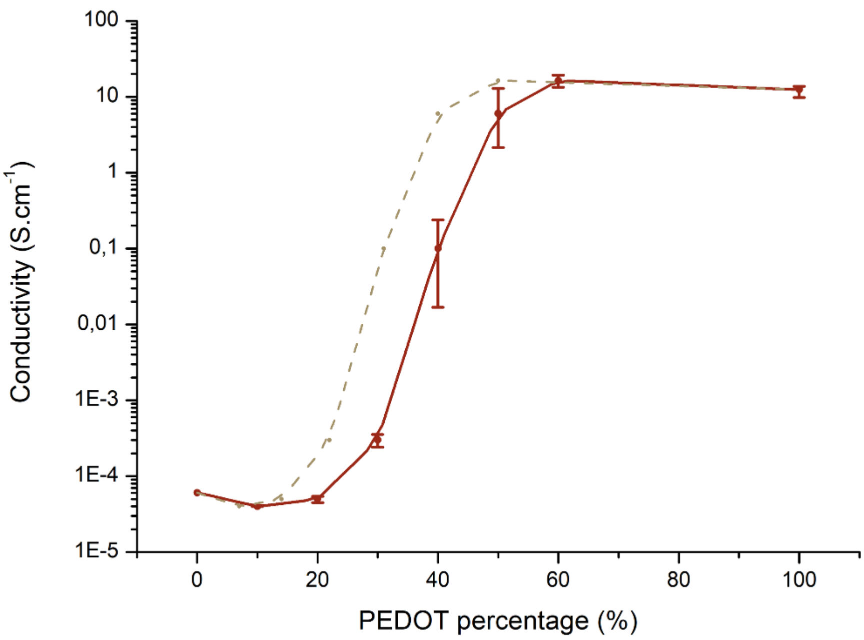

Figure 9: Evolution of the electrical conductivity of PEO / PEDOT thermoplastic composites as a function of the PEDOT weight content (red) or PEDOT volume content (dash line).

A particular attention was subsequently paid to the electrical percolation threshold in PEO / PEDOT thermoplastic composites. The electrical percolation threshold is obviously higher that 20 wt% of PEDOT and a quantitative value was extracted from experimental electrical conductivities using a classical scaling law (**Equation 6**) [33].

$$\sigma = \sigma_0(p - p_c)^t \qquad (6)$$

with p the volume fraction of PEDOT particles, p_c the electrical percolation threshold of the system, σ_0 a scaling factor depending on the electrical conductivity of PEDOT particles and t a critical exponent depending on the dimensionality of the system.

The density of PEDOT particles was evaluated to 1.7 g/cm^3 by pycnometry and weight fraction were converted into volume fraction. The best fit for current PEO / PEDOT thermoplastic composites gives an electrical percolation threshold pc close to 30 vol%, a critical exponent t close to 1.4 and a scaling factor σ_0 close to 100 S.cm^{-1}. The scaling factor σ_0 seems in good agreement with the electrical conductivity of PEDOT particles and the critical exponent t could indicate a dimensionality of the system close to 2, *i.e.* a 2D-electrical conductivity, a phenomenon potentially related to the 4-probe electrical measurement technique and / or a surface enrichment in PEDOT particles during die extrusion. Concerning the electrical percolation threshold, the critical volume fraction for equal-sized randomly packed hard spheres lies to 18.3% with a maximal packing density of 0.59 [73]. In this respect, our percolation threshold is significantly higher than the theoretical one. This effect can be potentially ascribed to the non-spherical shape of PEDOT particles but also to a non-statistical dispersion of PEDOT particles inside the PEO matrix (heterogenous dispersion and presence of aggregates / agglomerates). A morphological analysis was thus subsequently conducted to evaluate the dispersion quality of PEDOT particles in the PEO matrix by twin-screw extrusion.

3.5. Morphology of PEO / PEDOT composites manufactured by extrusion

The morphology of PEO / PEDOT thermoplastic composites was consequently analysed by SEM and X-ray tomography in order to detect the dispersion state of PEDOT into the PEO matrix by twin-screw extrusion. SEM analysis was performed on extruded ribbons after a cryogenic and fragile rupture perpendicular to the extrusion direction in order to properly reveal their transversal cross-sections (**Figure 10**). In these preparation conditions, pure PEO displays smooth and homogenous cross-sections typically observed with fragile ruptures. The incorporation of PEDOT induce strong modifications in the cryogenic fracture mechanism and PEDOT particles embedded in PEO are clearly observed. These morphological features attest for a very good adhesion between PEDOT particles and PEO. Concerning the dispersion state of PEDOT particles into PEO, SEM images seem to show that the best dispersion state is obtained with 10wt% of PEDOT particles. Individual PEDOT particles with diameters down to approx. 2 µm are observed and compared to the morphology / size of initial PEDOT particles (**Figure 4**) ; the twin-screw extrusion step seems to be quite efficient to break down initial "cauliflower"-like PEDOT particles into smaller particles. For PEDOT content higher than 20 wt%, the presence of PEDOT aggregates / agglomerates is clearly detected and these observations are consistent with percolation threshold higher than the theoretical one. However, SEM images are not able to reveal a percolation between PEDOT particles, even at elevated PEDOT content. In this respect, extruded ribbons were also analysed by X-ray tomography and the obtained 3D tomographic images of cross-sections are displayed in **Figure 11**. It could be first noticed in these images that the density difference between PEO (approx. 1.25 g/cm^3) and PEDOT (approx. 1.7 g/cm^3) is quite significant but too small to be detected by X-Ray tomography. The contrast observed in 3D tomographic images is believed to arise from iron(II) sulfate located inside PEDOT particles and the contrast could be here used to determine the location of PEDOT particles inside extruded ribbons but no information regarding the size of PEDOT particles could be extracted. 3D-tomographic images are quite consistent with SEM analyses. A very good dispersion state of PEDOT particles into the PEO matrix is attested for 10 wt% PEDOT. The dispersion is less efficient for higher PEDOT contents and a surface segregation phenomenon is observed for extreme PEDOT content (approx. 50 wt%). Interestingly, 3D tomographic images could detect the percolation of PEDOT particles. For 10 – 20 wt% PEDOT, no percolation between PEDOT particles is observed but, for PEDOT content higher than 30 wt%, a percolation path can be envisioned. 3D-tomograhic images consequently confirm the percolation threshold close to 30 wt% PEDOT in current composites produced by twin-screw extrusion. As a conclusion, a good adhesion and dispersion state of PEDOT particles into PEO is observed. Twin-screw extrusion could efficiently break down and disperse initial irregular PEDOT particles into smaller ones. However, the efficiency is less pronounced at elevated PEDOT content and initial aggregates / agglomerates of PEDOT currently persist after twin-screw extrusion. This phenomenon could largely explain the current electrical percolation threshold observed in PEO / PEDOT thermoplastic composites, a percolation that could be revealed by X-Ray tomography.

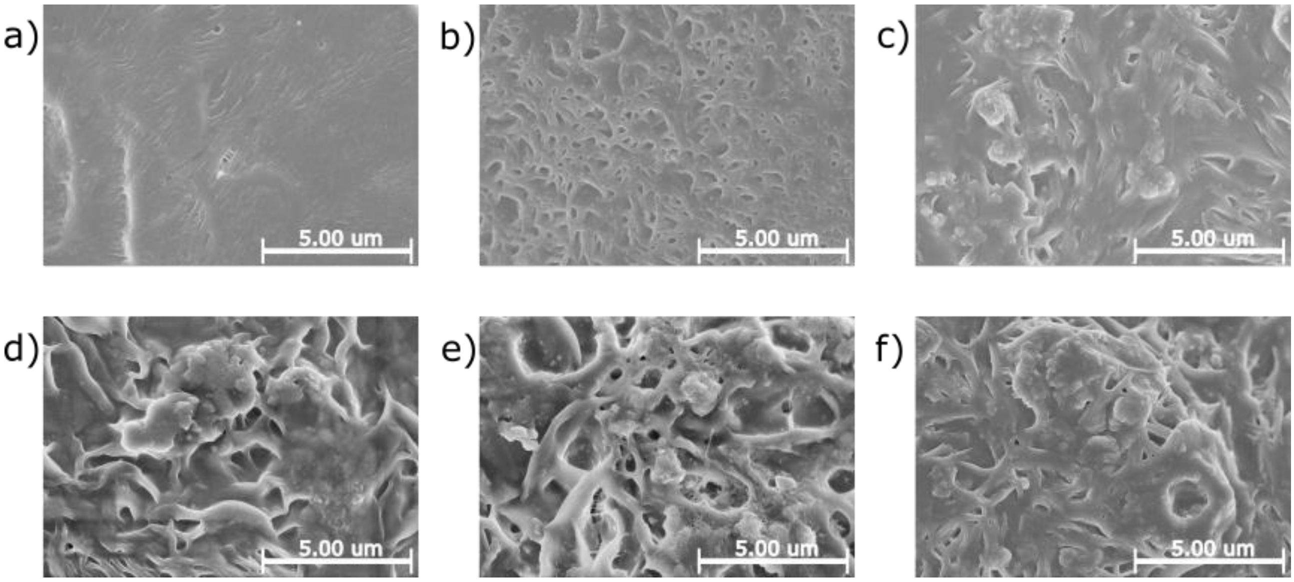

Figure 10: Morphology of PEO / PEDOT thermoplastic composites observed by SEM: (a) pure PEO, (b) 10 wt% PEDOT, (c) 20 wt% PEDOT, (d) 30 wt% PEDOT, (e) 40 wt% PEDOT and (d) 50 wt% PEDOT.

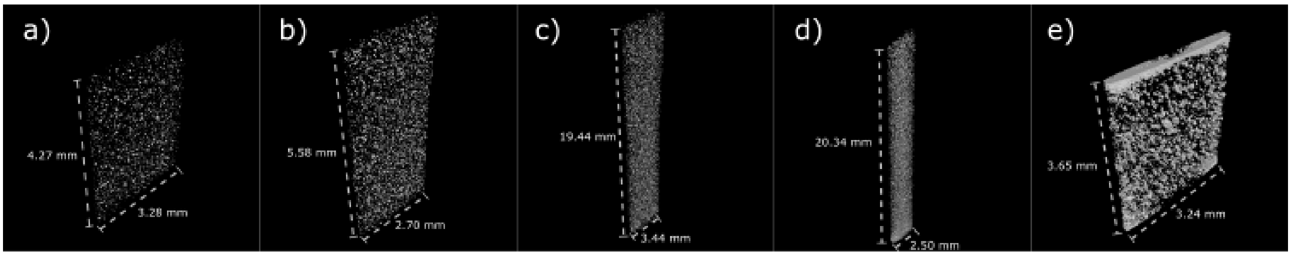

Figure 11: X-Ray tomography of PEO / PEDOT thermoplastic composites: (a) 10 wt% PEDOT, (b) 20 wt% PEDOT, (c) 30 wt% PEDOT, (d) 40 wt% PEDOT and (e) 50 wt% PEDOT.

3.6. Thermal properties of PEO / PEDOT composites manufactured by extrusion

Thermal properties of PEO / PEDOT thermoplastic composites were also examined with a specific focus on the crystallization / melting of PEO in order to detect the impact of PEDOT. Thermograms in the range 30 – 60°C are displayed in **Figure 12**. The crystallization of PEO from the melt state is clearly detected on the cooling scan and the melting of as-produced PEO crystals is then observed during the second heating scan. Pure PEO displays a crystallization temperature close to 43.8°C for a subsequent melting temperature close to 65°C (**Table 4**). PEO is a highly-crystalline material with a degree of crystallinity close to 75%, in accordance with many studies on this subject [74]. The incorporation of 10 – 20 wt% of PEDOT particles in PEO only produces minor modifications of the crystallization / melting temperatures by less than 1°C. The degree of crystallinity of PEO also remains close to 75% in these composites. However, for PEDOT content higher than 30 wt%, strong modifications in the PEO crystallization / melting temperatures are observed. The crystallization temperature of PEO decreases by approx. 4°C and the melting temperature by 6°C in PEO / PEDOT composites with 40 – 50 wt% PEDOT. The degree of crystallinity also decreases to approx. 70% and these elements indicate that PEDOT particles tend to reduce the crystallization rate of PEO. Similar effects have been previously detected for PEO / PEDOT:PSS blends and attributed to strong interactions in these compatible systems [51]. Other assumption are also plausible, in particular a PEO degradation in the melt state in the presence of PEDOT particles and their related impurities.

Table 4: PEO melting temperature, melting enthalpy and crystallinity as a function of the PEDOT content in PEO / PEDOT thermoplastic composites produced by twin-screw extrusion (DSC analysis, second heating scan).

PEDOT content (wt%)	PEO melting temperature (°C)	PEO melting enthalpy (J/g)	PEO crystallinity (%)
0	65.0	157.0	75
10	64.1	154.5	74
20	64.1	159.8	76
30	60.5	152.3	73
40	58.7	151.8	73
50	59.1	145.3	70

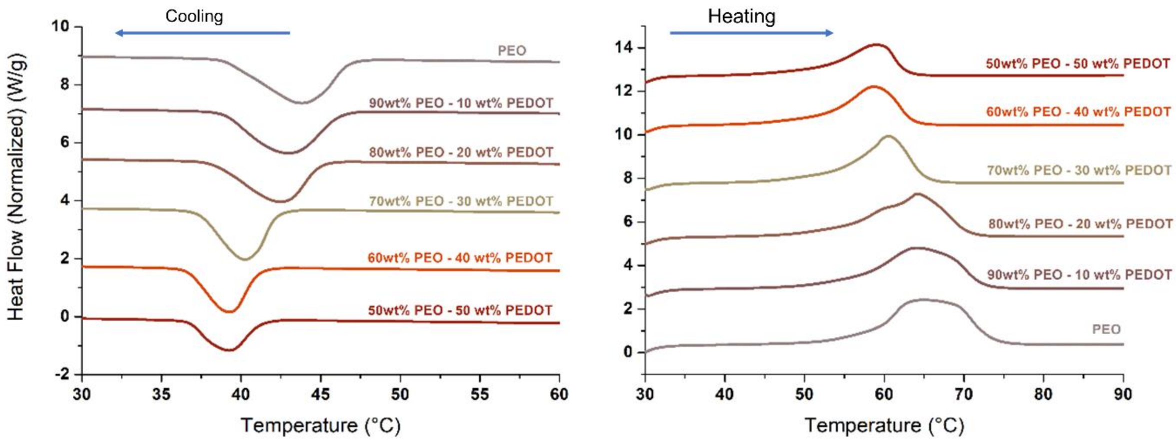

Figure 12: Thermograms of PEO / PEDOT thermoplastic composites produced by twin-screw extrusion. Cooling curves from the melt state (left) and second heating curves (right) as a function of the PEO content.

Finally, a highly conductive material was obtained by extrusion, with conductivities higher than 10 $S.cm^{-1}$. However, these conductivities are obtained with a high charge rate what leads to an extrudable material which is relatively brittle. For this reason, it is important to consider a diminution of the charge rate to avoid obtaining a brittle material. In the literature, the influence of the aspect ratio of the conductive filler on the percolation threshold has been clearly demonstrated [75]. Further studies need to be realised to improve the aspect ratio of the PEDOT conductive fillers in order to reduce drastically the percolation threshold.

4. CONCLUSIONS

Electrically-conductive PEDOT particles (without PSS) were successfully produced and this new type of micron-sized filler was used for the manufacture of electrically-conductive PEO / PEDOT thermoplastic composites by twin-screw extrusion. To the best of our knowledge, this study represents the first report about electrically-conductive thermoplastic composites based on PEDOT particles instead of traditional metallic or carbon-based fillers.

The production of micron-sized PEDOT particles (suitable for extrusion processing) with electrical conductivities as high as 50 S/cm was quite straightforward using an oxidative polymerization process of EDOT in water at room temperature. The polymerization temperature was found to be the most critical polymerization parameter to control the electrical conductivity of PEDOT particles. The best electrical conductivity is obtained at low polymerization temperatures (close to room temperature) while high polymerization temperatures dramatically reduce the electrical properties. Structural features controlling the electrical properties of PEDOT particles were tested. According to XRD / XPS analysis, the crystalline structuration of PEDOT particles seems to be of prime importance (*i.e.* size / amount of the PEDOT crystals, lamellar stacking distance, etc…). The presence of iron(II) sulfate impurities could also limit the electrical properties of PEDOT particles.

The incorporation of PEDOT particles into PEO was possible for up to 60 wt% by twin-screw extrusion. The electrical percolation was found close to 30 vol% of PEDOT. These results are in accordance with a percolation model for equal-sized randomly packed hard spheres, except that the observed percolation threshold is slightly higher than the theoretical model. This effect is ascribed to the dispersion state of PEDOT particles. At low PEDOT content (10 – 20 wt%), the twin-screw extrusion process is able to break down initial PEDOT aggregates / agglomerates into smaller and well-dispersed particles. Residual aggregates / agglomerates seem to persist for higher PEDOT content. However, as-produced PEO / PEDOT thermoplastic composites could display outstanding electrical conductivity up to 12 S/cm.

To the best of our knowledge, this value is one of the highest electrical conductivities reported in the open literature for thermoplastic composites manufactured by a melt-state technology. Many ongoing challenges are noticed (such as the improvement of the electrical properties of PEDOT particles and the modification of the electrical percolation threshold in PEDOT-based thermoplastic composites) but this work clearly opens up interesting scientific and technological perspectives for this new type of thermoplastic composites.

Acknowledgments

All authors acknowledge the DIFFERIX platform (Doru Constantin, Guillaume Fleith and Jérome Combet) for the XRD measurements and data analysis. Authors acknowledge the SOLEIL platform for the provision of synchrotron radiation facilities and Thomas Bizien for assistance in using the SWING beamline. Authors acknowledge the MINAMEC platform (Antoine Egele) for conductivity measurements, X-ray tomography and data interpretation. Authors especially acknowledge Damien Favier for the realisation of the four probes conductivity measurement device. Authors acknowledge the PLAMICS microscopy facility of ICS. Authors acknowledge Vasiliki Papaefthymiou for XPS measurements and his precious help on data interpretation.

CS and JS particularly acknowledge the Wallonia Region / Service Public de Wallonie (Belgium), West Vlaanderen Region (Belgium), Agentschap Innoveren Ondernemen (Belgium) and European Commission (FEDER) for the financial support regarding important chemicals in the framework of the INTERREG France─Wallonie─Vlaanderen program (BIOHARV project, GoToS3 portofolio).

References:

[1] J. Amarasekera, “Conductive plastics for electrical and electronic applications,” *Reinforced Plastics*, vol. 49, no. 8, pp. 38–41, Sep. 2005, doi: 10.1016/S0034-3617(05)70734-7.

[2] J.-C. Huang, “Carbon black filled conducting polymers and polymer blends,” *Advances in Polymer Technology*, vol. 21, no. 4, pp. 299–313, 2002, doi: 10.1002/adv.10025.

[3] S. K. H. Gulrez *et al.*, “A review on electrically conductive polypropylene and polyethylene,” *Polym Compos*, vol. 35, no. 5, pp. 900–914, May 2014, doi: 10.1002/pc.22734.

[4] M. Narkis, G. Lidor, A. Vaxman, and L. Zuri, “Novel Electrically Conductive Injection Moldable Thermoplastic Composites For ESD Applications,” in *Conductive Polymers and Plastics*, Elsevier, 1999, pp. 209–217. doi: 10.1016/B978-188420777-8.50030-8.

[5] R. B. Rosner, “Conductive materials for ESD applications: an overview,” in *Electrical Overstress/Electrostatic Discharge Symposium Proceedings 2000 (IEEE Cat. No.00TH8476)*, ESD Assoc, 2000, pp. 121–131. doi: 10.1109/EOSESD.2000.890035.

[6] L. de Souza Vieira *et al.*, “Carbon-based materials as antistatic agents for the production of antistatic packaging: a review,” *Journal of Materials Science: Materials in Electronics*, vol. 32, no. 4, pp. 3929–3947, Feb. 2021, doi: 10.1007/s10854-020-05178-6.

[7] L. Rupprecht, “Conductive Thermoplastic Compounds for EMI/RFI Applications,” in *Conductive Polymers and Plastics*, Elsevier, 1999, pp. 143–152. doi: 10.1016/B978-188420777-8.50021-7.
[8] K. Shahapurkar *et al.*, “Comprehensive review on polymer composites as electromagnetic interference shielding materials,” *Polymers and Polymer Composites*, vol. 30, p. 096739112211021, Jan. 2022, doi: 10.1177/09673911221102127.
[9] J. Kruželák, A. Kvasničáková, K. Hložeková, and I. Hudec, “Progress in polymers and polymer composites used as efficient materials for EMI shielding,” *Nanoscale Adv*, vol. 3, no. 1, pp. 123–172, 2021, doi: 10.1039/D0NA00760A.
[10] S. Geetha, K. K. Satheesh Kumar, C. R. K. Rao, M. Vijayan, and D. C. Trivedi, “EMI shielding: Methods and materials-A review,” *J Appl Polym Sci*, vol. 112, no. 4, pp. 2073–2086, May 2009, doi: 10.1002/app.29812.
[11] S. Sankaran, K. Deshmukh, M. B. Ahamed, and S. K. Khadheer Pasha, “Recent advances in electromagnetic interference shielding properties of metal and carbon filler reinforced flexible polymer composites: A review,” *Compos Part A Appl Sci Manuf*, vol. 114, pp. 49–71, Nov. 2018, doi: 10.1016/j.compositesa.2018.08.006.
[12] B. Wang and A. Facchetti, “Mechanically Flexible Conductors for Stretchable and Wearable E-Skin and E-Textile Devices,” *Advanced Materials*, vol. 31, no. 28, p. 1901408, Jul. 2019, doi: 10.1002/adma.201901408.
[13] H. Liu *et al.*, “Electrically conductive polymer composites for smart flexible strain sensors: a critical review,” *J Mater Chem C Mater*, vol. 6, no. 45, pp. 12121–12141, 2018, doi: 10.1039/C8TC04079F.
[14] J. Chen *et al.*, “Advances in Responsively Conductive Polymer Composites and Sensing Applications,” *Polymer Reviews*, vol. 61, no. 1, pp. 157–193, Jan. 2021, doi: 10.1080/15583724.2020.1734818.
[15] F. Badrul, K. A. A. Halim, M. A. A. M. Salleh, M. F. Omar, A. F. Osman, and M. S. Zakaria, “Current advancement in electrically conductive polymer composites for electronic interconnect applications: A short review,” *IOP Conf Ser Mater Sci Eng*, vol. 701, no. 1, p. 012039, Dec. 2019, doi: 10.1088/1757-899X/701/1/012039.
[16] R. Olejník, S. Goňa, P. Slobodian, J. Matyáš, R. Moučka, and R. Daňová, “Polyurethane-Carbon Nanotubes Composite Dual Band Antenna for Wearable Applications,” *Polymers (Basel)*, vol. 12, no. 11, p. 2759, Nov. 2020, doi: 10.3390/polym12112759.
[17] O. A. Alo, I. O. Otunniyi, and E. R. Sadiku, “Processing methods for conductive polymer composite bipolar plates: Effect on plate quality and performance,” *Fuel Cells*, Jan. 2023, doi: 10.1002/fuce.202100157.
[18] E. Planes, L. Flandin, and N. Alberola, “Polymer Composites Bipolar Plates for PEMFCs,” *Energy Procedia*, vol. 20, pp. 311–323, 2012, doi: 10.1016/j.egypro.2012.03.031.
[19] A. Hermann, T. Chaudhuri, and P. Spagnol, “Bipolar plates for PEM fuel cells: A review,” *Int J Hydrogen Energy*, vol. 30, no. 12, pp. 1297–1302, Sep. 2005, doi: 10.1016/j.ijhydene.2005.04.016.
[20] A. Abdisattar *et al.*, “Recent advances and challenges of current collectors for supercapacitors,” *Electrochem commun*, vol. 142, p. 107373, Sep. 2022, doi: 10.1016/j.elecom.2022.107373.
[21] N. Verdier, G. Foran, D. Lepage, A. Prébé, D. Aymé-Perrot, and M. Dollé, “Challenges in Solvent-Free Methods for Manufacturing Electrodes and Electrolytes for Lithium-Based Batteries,” *Polymers (Basel)*, vol. 13, no. 3, p. 323, Jan. 2021, doi: 10.3390/polym13030323.

[22] L. Wang *et al.*, “Polymer composites-based thermoelectric materials and devices,” *Compos B Eng*, vol. 122, pp. 145–155, Aug. 2017, doi: 10.1016/j.compositesb.2017.04.019.

[23] A. Dey, O. P. Bajpai, A. K. Sikder, S. Chattopadhyay, and M. A. Shafeeuulla Khan, “Recent advances in CNT/graphene based thermoelectric polymer nanocomposite: A proficient move towards waste energy harvesting,” *Renewable and Sustainable Energy Reviews*, vol. 53, pp. 653–671, Jan. 2016, doi: 10.1016/j.rser.2015.09.004.

[24] S. Agarwala, G. L. Goh, G. D. Goh, V. Dikshit, and W. Y. Yeong, “3D and 4D printing of polymer/CNTs-based conductive composites,” in *3D and 4D Printing of Polymer Nanocomposite Materials*, Elsevier, 2020, pp. 297–324. doi: 10.1016/B978-0-12-816805-9.00010-7.

[25] M. V. C. Morais, R. Reidel, P. Weiss, S. Baumann, C. Hubner, and F. Henning, “Integration of electronic components in the thermoplastic processing chain: possibilities through additive manufacturing using conductive materials,” in *2018 13th International Congress Molded Interconnect Devices (MID)*, IEEE, Sep. 2018, pp. 1–4. doi: 10.1109/ICMID.2018.8527054.

[26] X. Yan, Y. Tong, X. Wang, F. Hou, and J. Liang, “Extrusion-Based 3D-Printed Supercapacitors: Recent Progress and Challenges,” *ENERGY & ENVIRONMENTAL MATERIALS*, vol. 5, no. 3, pp. 800–822, Jul. 2022, doi: 10.1002/eem2.12260.

[27] J. F. Christ, N. Aliheidari, A. Ameli, and P. Pötschke, “3D printed highly elastic strain sensors of multiwalled carbon nanotube/thermoplastic polyurethane nanocomposites,” *Mater Des*, vol. 131, pp. 394–401, Oct. 2017, doi: 10.1016/j.matdes.2017.06.011.

[28] K. Kim, J. Park, J. Suh, M. Kim, Y. Jeong, and I. Park, “3D printing of multiaxial force sensors using carbon nanotube (CNT)/thermoplastic polyurethane (TPU) filaments,” *Sens Actuators A Phys*, vol. 263, pp. 493–500, Aug. 2017, doi: 10.1016/j.sna.2017.07.020.

[29] C. J. Hohimer, G. Petrossian, A. Ameli, C. Mo, and P. Pötschke, “3D printed conductive thermoplastic polyurethane/carbon nanotube composites for capacitive and piezoresistive sensing in soft pneumatic actuators,” *Addit Manuf*, vol. 34, p. 101281, Aug. 2020, doi: 10.1016/j.addma.2020.101281.

[30] A. Maurel *et al.*, “Highly Loaded Graphite–Polylactic Acid Composite-Based Filaments for Lithium-Ion Battery Three-Dimensional Printing,” *Chemistry of Materials*, vol. 30, no. 21, pp. 7484–7493, Nov. 2018, doi: 10.1021/acs.chemmater.8b02062.

[31] N. A. Mohd Radzuan, A. B. Sulong, and J. Sahari, “A review of electrical conductivity models for conductive polymer composite,” *Int J Hydrogen Energy*, vol. 42, no. 14, pp. 9262–9273, Apr. 2017, doi: 10.1016/j.ijhydene.2016.03.045.

[32] H. Deng, L. Lin, M. Ji, S. Zhang, M. Yang, and Q. Fu, “Progress on the morphological control of conductive network in conductive polymer composites and the use as electroactive multifunctional materials,” *Prog Polym Sci*, vol. 39, no. 4, pp. 627–655, Apr. 2014, doi: 10.1016/j.progpolymsci.2013.07.007.

[33] W. Bauhofer and J. Z. Kovacs, “A review and analysis of electrical percolation in carbon nanotube polymer composites,” *Compos Sci Technol*, vol. 69, no. 10, pp. 1486–1498, Aug. 2009, doi: 10.1016/j.compscitech.2008.06.018.

[34] R. Sengupta, M. Bhattacharya, S. Bandyopadhyay, and A. K. Bhowmick, “A review on the mechanical and electrical properties of graphite and modified graphite reinforced polymer composites,” *Prog Polym Sci*, vol. 36, no. 5, pp. 638–670, May 2011, doi: 10.1016/j.progpolymsci.2010.11.003.

[35] A. J. Marsden *et al.*, “Electrical percolation in graphene–polymer composites,” *2d Mater*, vol. 5, no. 3, p. 032003, Jun. 2018, doi: 10.1088/2053-1583/aac055.
[36] J. Sanes, C. Sánchez, R. Pamies, M.-D. Avilés, and M.-D. Bermúdez, “Extrusion of Polymer Nanocomposites with Graphene and Graphene Derivative Nanofillers: An Overview of Recent Developments,” *Materials*, vol. 13, no. 3, p. 549, Jan. 2020, doi: 10.3390/ma13030549.
[37] M. N. Gueye, A. Carella, J. Faure-Vincent, R. Demadrille, and J.-P. Simonato, “Progress in understanding structure and transport properties of PEDOT-based materials: A critical review,” *Prog Mater Sci*, vol. 108, p. 100616, Feb. 2020, doi: 10.1016/j.pmatsci.2019.100616.
[38] C. Wang *et al.*, “Enhancement of Conductivity and Thermoelectric Property of PEDOT:PSS via Acid Doping and Single Post-Treatment for Flexible Power Generator,” *Adv Sustain Syst*, vol. 2, no. 12, p. 1800085, Dec. 2018, doi: 10.1002/adsu.201800085.
[39] A. Schultheiss *et al.*, “Water content control during solution-based polymerization: a key to reach extremely high conductivity in PEDOT thin films,” *J Mater Chem C Mater*, vol. 8, no. 48, pp. 17254–17260, 2020, doi: 10.1039/D0TC04899B.
[40] H. Shi, C. Liu, Q. Jiang, and J. Xu, “Effective Approaches to Improve the Electrical Conductivity of PEDOT:PSS: A Review,” *Adv Electron Mater*, vol. 1, no. 4, p. 1500017, Apr. 2015, doi: 10.1002/aelm.201500017.
[41] X. Fan *et al.*, “PEDOT:PSS for Flexible and Stretchable Electronics: Modifications, Strategies, and Applications,” *Advanced Science*, vol. 6, no. 19, p. 1900813, Oct. 2019, doi: 10.1002/advs.201900813.
[42] J. Lu *et al.*, “Ultrathin PEDOT:PSS Enables Colorful and Efficient Perovskite Light-Emitting Diodes,” *Advanced Science*, vol. 7, no. 11, p. 2000689, Jun. 2020, doi: 10.1002/advs.202000689.
[43] R. P. Ortiz, A. Facchetti, and T. J. Marks, “High-k Organic, Inorganic, and Hybrid Dielectrics for Low-Voltage Organic Field-Effect Transistors,” *Chem Rev*, vol. 110, no. 1, pp. 205–239, Jan. 2010, doi: 10.1021/cr9001275.
[44] D. Natali and M. Caironi, “Charge Injection in Solution-Processed Organic Field-Effect Transistors: Physics, Models and Characterization Methods,” *Advanced Materials*, vol. 24, no. 11, pp. 1357–1387, Mar. 2012, doi: 10.1002/adma.201104206.
[45] K. Sun *et al.*, “Review on application of PEDOTs and PEDOT:PSS in energy conversion and storage devices,” *Journal of Materials Science: Materials in Electronics*, vol. 26, no. 7, pp. 4438–4462, Jul. 2015, doi: 10.1007/s10854-015-2895-5.
[46] L. Hu, J. Song, X. Yin, Z. Su, and Z. Li, “Research Progress on Polymer Solar Cells Based on PEDOT:PSS Electrodes,” *Polymers (Basel)*, vol. 12, no. 1, p. 145, Jan. 2020, doi: 10.3390/polym12010145.
[47] C. Wang *et al.*, “Enhancement of Conductivity and Thermoelectric Property of PEDOT:PSS via Acid Doping and Single Post-Treatment for Flexible Power Generator,” *Adv Sustain Syst*, vol. 2, no. 12, p. 1800085, Dec. 2018, doi: 10.1002/adsu.201800085.
[48] Z. Fan and J. Ouyang, “Thermoelectric Properties of PEDOT:PSS,” *Adv Electron Mater*, vol. 5, no. 11, p. 1800769, Nov. 2019, doi: 10.1002/aelm.201800769.
[49] Y. Liang, A. Offenhäusser, S. Ingebrandt, and D. Mayer, “PEDOT:PSS-Based Bioelectronic Devices for Recording and Modulation of Electrophysiological and Biochemical Cell Signals,” *Adv Healthc Mater*, vol. 10, no. 11, p. 2100061, Jun. 2021, doi: 10.1002/adhm.202100061.

[50] G. E. Fenoy, O. Azzaroni, W. Knoll, and W. A. Marmisollé, “Functionalization Strategies of PEDOT and PEDOT:PSS Films for Organic Bioelectronics Applications,” *Chemosensors*, vol. 9, no. 8, p. 212, Aug. 2021, doi: 10.3390/chemosensors9080212.
[51] C. Duc, G. Stoclet, J. Soulestin, and C. Samuel, “Poly(ethylene oxide)/Poly(3,4-ethylenedioxythiophene):Poly(styrene sulfonate) (PEDOT:PSS) Blends: An Efficient Route to Highly Conductive Thermoplastic Materials for Melt-State Extrusion Processing ?,” *ACS Appl Polym Mater*, vol. 2, no. 6, pp. 2366–2379, Jun. 2020, doi: 10.1021/acsapm.0c00303.
[52] A. R. Hopkins and J. R. Reynolds, “Crystallization driven formation of conducting polymer networks in polymer blends,” *Macromolecules*, vol. 33, no. 14, pp. 5221–5226, 2000, doi: 10.1021/ma991347t.
[53] M. Kemerink, S. Timpanaro, M. M. De Kok, E. A. Meulenkamp, and F. J. Touwslager, “Three-dimensional inhomogeneities in PEDOT:PSS films,” *Journal of Physical Chemistry B*, vol. 108, no. 49, pp. 18820–18825, 2004, doi: 10.1021/jp0464674.
[54] C. Duc, G. Stoclet, J. Soulestin, and C. Samuel, “Poly(ethylene oxide)/Poly(3,4-ethylenedioxythiophene):Poly(styrene sulfonate) (PEDOT:PSS) Blends: An Efficient Route to Highly Conductive Thermoplastic Materials for Melt-State Extrusion Processing ?,” *ACS Appl Polym Mater*, vol. 2, no. 6, pp. 2366–2379, Jun. 2020, doi: 10.1021/acsapm.0c00303.
[55] C. Jiang, G. Chen, and X. Wang, “High-conversion synthesis of poly(3,4-ethylenedioxythiophene) by chemical oxidative polymerization,” *Synth Met*, vol. 162, no. 21–22, pp. 1968–1971, 2012, doi: 10.1016/j.synthmet.2012.09.008.
[56] H. Topsoe, “Geometric factors in four point resistivity measurement.” 1966.
[57] C. Jiang, G. Chen, and X. Wang, “High-conversion synthesis of poly(3,4-ethylenedioxythiophene) by chemical oxidative polymerization,” *Synth Met*, vol. 162, no. 21–22, pp. 1968–1971, 2012, doi: 10.1016/j.synthmet.2012.09.008.
[58] G. Cao, S. Cai, Y. Chen, D. Zhou, H. Zhang, and Y. Tian, “Facile synthesis of highly conductive and dispersible PEDOT particles,” *Polymer (Guildf)*, vol. 252, no. March, p. 124952, Jun. 2022, doi: 10.1016/j.polymer.2022.124952.
[59] N. Paradee and A. Sirivat, “Synthesis of poly(3,4-ethylenedioxythiophene) nanoparticles via chemical oxidation polymerization,” *Polym Int*, vol. 63, no. 1, pp. 106–113, 2014, doi: 10.1002/pi.4538.
[60] C. Jiang, G. Chen, and X. Wang, “High-conversion synthesis of poly(3,4-ethylenedioxythiophene) by chemical oxidative polymerization,” *Synth Met*, vol. 162, no. 21–22, pp. 1968–1971, 2012, doi: 10.1016/j.synthmet.2012.09.008.
[61] K. E. Aasmundtveit, E. J. Samuelsen, L. A. A. Pettersson, O. Inganäs, T. Johansson, and R. Feidenhans’l, “Structure of thin films of poly(3,4-ethylenedioxythiophene),” *Synth Met*, vol. 101, no. 1, pp. 561–564, 1999, doi: 10.1016/S0379-6779(98)00315-4.
[62] N. Massonnet, A. Carella, A. de Geyer, J. Faure-Vincent, and J.-P. Simonato, “Metallic behaviour of acid doped highly conductive polymers,” *Chem Sci*, vol. 6, no. 1, pp. 412–417, 2015, doi: 10.1039/C4SC02463J.
[63] M. N. Gueye *et al.*, “Structure and Dopant Engineering in PEDOT Thin Films: Practical Tools for a Dramatic Conductivity Enhancement,” *Chemistry of Materials*, vol. 28, no. 10, pp. 3462–3468, May 2016, doi: 10.1021/acs.chemmater.6b01035.
[64] E. C. Sklute, H. B. Jensen, A. D. Rogers, and R. J. Reeder, “Morphological, structural, and spectral characteristics of amorphous iron sulfates,” *Nature*, vol. 175, no. 4449, p. 238, 1955, doi: 10.1038/175238c0.

[65] A. Van Alboom, V. G. De Resende, E. De Grave, and J. A. M. Gómez, “Hyperfine interactions in szomolnokite (FeSO4·H2O),” *J Mol Struct*, vol. 924–926, no. C, pp. 448–456, 2009, doi: 10.1016/j.molstruc.2008.10.049.

[66] M. Lacalamita, G. Ventruti, G. della Ventura, F. Radica, D. Mauro, and E. Schingaro, “In Situ High-Temperature X-ray Powder Diffraction and Infrared Spectroscopic Study of Melanterite, FeSO4·7H2O,” *Minerals*, vol. 11, no. 4, p. 392, Apr. 2021, doi: 10.3390/min11040392.

[67] G. Zotti *et al.*, “Electrochemical and XPS Studies toward the Role of Monomeric and Polymeric Sulfonate Counterions in the Synthesis, Composition, and Properties of Poly(3,4-ethylenedioxythiophene),” *Macromolecules*, vol. 36, no. 9, pp. 3337–3344, May 2003, doi: 10.1021/ma021715k.

[68] I. Ivanko, J. Svoboda, M. Lukešová, I. Šeděnková, and E. Tomšík, “Hydrogen Bonding as a Tool to Control Chain Structure of PEDOT: Electrochemical Synthesis in the Presence of Different Electrolytes,” *Macromolecules*, vol. 53, no. 7, pp. 2464–2473, Apr. 2020, doi: 10.1021/acs.macromol.9b02627.

[69] W. W. Chiu, J. Travaš-Sejdić, R. P. Cooney, and G. A. Bowmaker, “Spectroscopic and conductivity studies of doping in chemically synthesized poly(3,4-ethylenedioxythiophene),” *Synth Met*, vol. 155, no. 1, pp. 80–88, Oct. 2005, doi: 10.1016/j.synthmet.2005.06.012.

[70] Khan M *et al.*, “Surface Characterization of Poly(3,4-ethylenedioxythiophene)-Coated Latexes by X-ray Photoelectron Spectroscopy,” *Langmuir* , vol. 16, no. 9, pp. 4171–4179, 2000.

[71] I. Petsagkourakis *et al.*, “A nuanced understanding of the doping of poly(3,4-ethylenedioxythiophene) with tosylate,” *Discov Mater*, vol. 3, no. 1, 2023, doi: 10.1007/s43939-023-00046-6.

[72] V. Sethumadhavan, K. Zuber, C. Bassell, P. R. Teasdale, and D. Evans, “Hydrolysis of doped conducting polymers,” *Commun Chem*, vol. 3, no. 1, pp. 1–9, 2020, doi: 10.1038/s42004-020-00404-y.

[73] M. J. Powell, “Site percolation in randomly packed spheres,” *Phys Rev B*, vol. 20, no. 10, pp. 4194–4198, Nov. 1979, doi: 10.1103/PhysRevB.20.4194.

[74] Y. Hu, Y. S. Hu, V. Topolkaraev, A. Hiltner, and E. Baer, “Crystallization and phase separation in blends of high stereoregular poly(lactide) with poly(ethylene glycol),” *Polymer (Guildf)*, vol. 44, no. 19, pp. 5681–5689, 2003, doi: 10.1016/S0032-3861(03)00609-8.

[75] Jérémie AUDOIT, “Optimisation de la conductivité électrique transverse de composites structuraux PAEK–fils submicroniques d’argent / fibres de carbone continues avec ensimage conducteur,” p. 147, 2017, [Online]. Available: http://thesesups.ups-tlse.fr/3432/1/2017TOU30001.pdf

Graphical Abstract

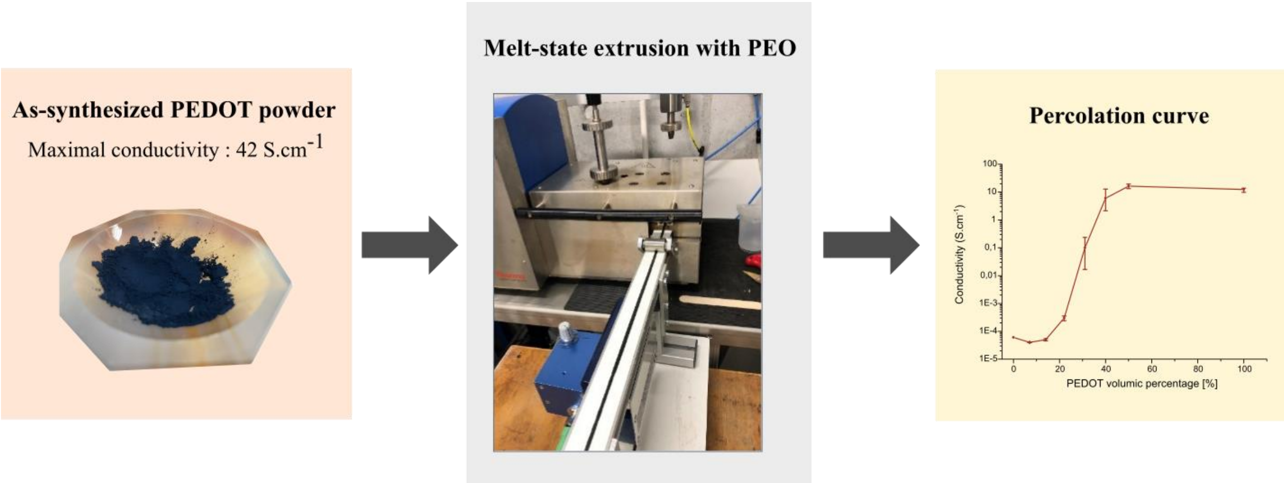
As-synthesized PEDOT powder
Maximal conductivity : 42 S.cm-1
Melt-state extrusion with PEO
Percolation curve
Conductivity (S.cm-1)
PEDOT volumic percentage [%]